Progress In Electromagnetics Research, PIER 22, 231–258, 1999

ANALYSIS OF RECTANGULAR WAVEGUIDES AND THICK WINDOWS AS EMI SENSORS

A. Bhattacharya, S. Gupta, and A. Chakraborty

Dept. of Electronics & Electrical Communication Engineering
Indian Institute of Technology
Kharagpur-721 302, India

1. INTRODUCTION

All the electronic devices must conform to the standards of electromagnetic emission set by different bodies in different countries. The frequency range of conducted emission standards extend from 450 KHz to 30 MHz and that for radiated emissions begins at 30 MHz and extends to 40 GHz [1]. Compliance of the devices conforming to the standards (limits) of interference in this range is verified by measuring the radiated electric fields in an anechoic chamber or at an open test range after putting the measurement antenna at a specified distance from the device under test.

The measurement antennas or EMI sensors, in common use, are dipoles or loop antennas (e.g., EMI probe kit MA 8611A, EMI probe MA 2601 B/C of Anritsu Corporation, Japan), but unfortunately they are effective only up to a frequency of 1 GHz. Beyond this range, no

compact probe for EMI measurements has come to the notice either through journal publication or through product catalogues.

Open-end of a rectangular waveguide can be used very effectively as an EMI sensor, for frequency above 2 GHz. These sensors require a calibration data relating the voltage sensed at the matched detector with the electric field at the receiving aperture of the sensor. This relationship is often described by the Antenna Factor, which is defined as the ratio of the incident electric field at the surface of the sensing antenna to the received voltage at the antenna terminal [1]. In EMI measurements, it is, therefore, extremely important to know the antenna factor of the probe at each frequency, in order to determine the field strength at any point of measurement. This calibration requires extremely rigorous and expensive experiments. In this paper, an alternative in the form of a moment method procedure has been evolved to theoretically predict the antenna factor of the open-ended rectangular waveguide and window sensors. The computer aided evaluation of the antenna factor of sensors is a better alternative than experimental calibration of sensors because this can bypass the need of setting up of expensive calibration equipment and also saves a lot of time in calibrating a sensor. Also, computer aided calibration can take care of a variety of sensors much easily than manual calibration, because only the input to the software need to be changed.

The generalized analysis of a rectangular open-ended waveguide, particularly the analysis of a window radiator by using M.O.M. is being reported recently [2, 3]. An electromagnetic wave incident on the window or the open-end of the waveguide causes an electric field to be induced at the plane of the window/open-end of the waveguide, which satisfies the boundary conditions imposed by the geometry of the waveguide. The choice of global sinusoidal basis function for aperture antenna problems give fast convergence in Method of Moments formulation [9]. Hence, in the present approach, the unknown aperture field is described by a sum of M number of weighted sinusoidal basis functions, defined over the extent of the window. Field is radiated into free space and scattered inside the waveguide by the equivalent magnetic current source at the aperture. The tangential components of the scattered magnetic field within the waveguide and that radiated into the free space must be continuous at the plane of the aperture. Enforcement of this boundary condition leads to an integral equation involving the M unknowns used to describe the aperture electric field.

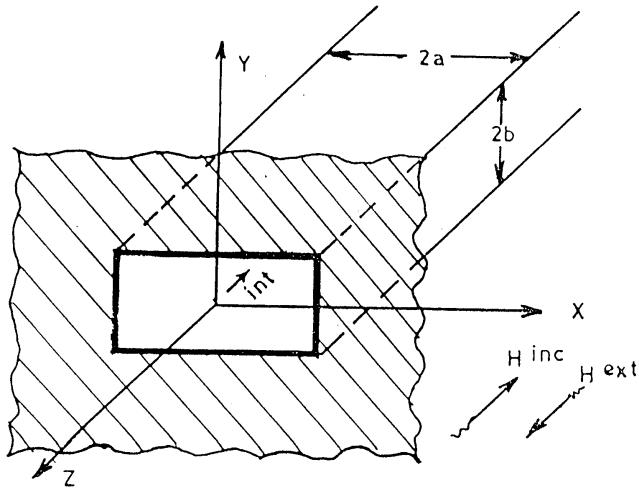

Figure 1. Open-ended of a rectangular waveguide as a receiving antenna.

This is transformed into matrix equation by taking moments with entire domain sinusoidal weighting function [3]. A solution of this matrix equation provides the values of the unknown coefficients. The field scattered inside the waveguide is obtained in terms of these coefficients. The component of the field due to the dominant TE_{10} mode is then obtained. Assuming a matched detector, the power received by the detector is obtained, from which the voltage at the measuring device is calculated. The relationship between the incident electric field and the measured voltage is thus theoretically established.

Measurements carried out for a window compare favorably with the theoretically predicted data. Experimental results obtained with open-ended waveguide probes with a ground plane of size reported in [3] agree very well with the computed results. It is felt that with better measuring environment. where stray reflections and other measuring inaccuracies can be minimized, an excellent agreement can very well be obtained. The theory and experiment matches well for different angle of incidence of the signal. Theoretical data is also presented for open-ended waveguide sensor with dielectric loading inside the waveguide.

2. ANALYSIS

2.1 Formulation of the Problem

The open-ended waveguide sensor can be seen in Figure 1. An incident electric field of intensity 1 Volt/meter is assumed to be incident on the aperture when a plane wave impinges at an angle θ_0 on the aperture. The following assumptions are made for simplifying the analysis [2–7]:

- The ground plane in Figure 1 is infinite in extent. Theoretically this assumption helps in evaluating the radiating field in a closed form expression. Experimentally it has been observed that the scattering parameters do start converging for ground planes of size $5\lambda \times 5\lambda$. So, in practice, the large (in terms of wavelength) ground plane taken satisfies the infinite ground plane assumption quite satisfactorily.
- The standard rectangular waveguide structures supports TE_{p0} modes near a discontinuity. Since all fields of this type are uniform in y direction and have a sinusoidal variation in the x-direction, the basis function for the aperture fields is also chosen similarly.
- For aspect ratios 2 and above, the aperture electric field variation to be described is quite justified.
- The aperture magnetic field lies in the X-Z plane and its X component is considered for satisfying the boundary condition. The cross polarized component of the magnetic field in the Y direction is neglected because in the absence of any nearby structure, cross polarized field is too small to be taken.

In general, the phase of the incoming electric field at any source point is given by,

$$e^{j\overline{k},\overline{r}'} = e^{j(k_x x' + k_y y' + k_z z')} \tag{1}$$

where k_x, k_y are related to the angle of incidence (θ_0, ϕ_0) as,

$$k_x = k \cos\theta_0 \cos\phi_0 \tag{2}$$

$$k_y = k \cos\theta_0 \sin\phi_0 \tag{3}$$

and $\overline{r}'$ is the radius vector of any source point and given by,

$$\overline{r}' = x'\hat{i} + y'\hat{j} \tag{4}$$

So, it is seen that the incident field from (θ_0, ϕ_0) direction introduces a relative phase at different points on the aperture when it falls on

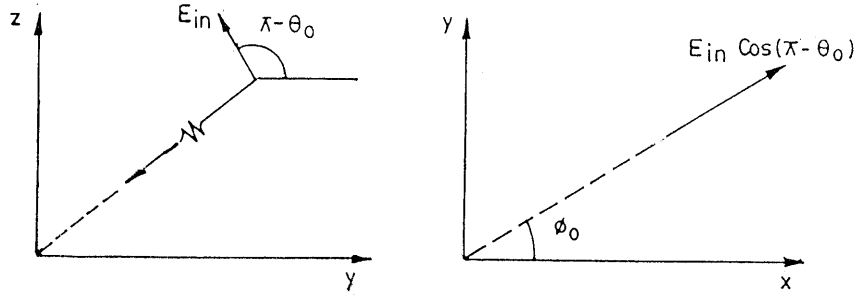

(a) (b)

Figure 2. (a) Incoming electric field in the y-z plane. (b) Projection of the incoming electric field in the x-y plane.

them. At the $Z = 0$ plane, the incident electric and magnetic field are given by the projection of the the incoming respective fields first in the X-Y plane as shown in Figure 2(a) and then by the projection in the respective axes as shown in Figure 2(b) So, incident electric field is given by

$$\overline{E}_{inc}(z=0) = -\left(\hat{u}_x \cos\theta_0 \cos\phi_0 + \hat{u}_y \cos\theta_0 \sin\phi_0\right) e^{j(k_x x' + k_y y')} \quad (5)$$

and incident magnetic field by

$$Y_o \overline{H}_{inc}(z=0) = \left(-\hat{u}_x \cos\theta_0 \sin\phi_0 + \hat{u}_y \cos\theta_0 \cos\phi_0\right) Y_0 e^{j(k_x x' + k_y y')} \quad (6)$$

where Y_o is the free space admittance.

For an incident wave coming from $\phi_0 = \pi/2$ direction,

- The aperture electric field can be described by

$$\vec{E}(x', y', 0) = \hat{u}_y \sum_{p=1}^{M} A_p e_p : \quad p = 1, 2, \ldots M \quad (7)$$

where the basis functions e_p are defined by,

$$e_p = \begin{cases} \sin\left\{\dfrac{p\pi}{2L}(x - x_w + L)\right\} & \begin{array}{c} x_{w-L} \le x \le x_{w+L} \\ y_w - w \le y \le y_w + w \end{array} \\ 0 & \text{elsewhere} \end{cases} \quad (8)$$

The choice of ϕ_0 in this case is arbitrary and chosen to make use of the analysis derived in [3] for the open-ended waveguide radiator case.

The open-ended waveguide receiver is the special case of the receiving window, when the window dimensions are the same as that of the waveguide, (x_w, y_w) refers to the center of the window with respect to the center of the face of the receiving waveguide.

- The externally and internally scattered magnetic field due to the assumed aperture field is evaluated by the following analysis given in [3].
- The boundary condition is obtained by decoupling the sources at the aperture and that incident from free space. The boundary condition can be written as,

$$H_x^{int} = 2H_x^{inc} + H_x^{ext} \tag{9}$$

- The weighting function is taken as

$$W_q(x', y', 0) = \begin{cases} \sin \dfrac{p\pi}{2L}(x' - x_w + L) & \begin{matrix} x_w - L \le x' \le x_w + L \\ Y_w - W \le y' \le Y_w + W \end{matrix} \\ 0 \end{cases} \tag{10}$$

The choice of same weighting function as basis function i.e., Galerkin's technique is a standard procedure in the Method of Moments procedure, as it reduces CPU time considerably in aperture problems [9]. The boundary condition is then solved to obtain the aperture basis coefficients A_p by the procedure identical to that described in [2, 3].

2.2 Antenna Factor

Although many modes are generated inside the waveguide near the aperture plane, the voltage is measured after the internally scattered wave travels several wavelengths inside the waveguide. This ensures that the measuring device receives only the dominant mode scattered power. So, the probe under consideration contains a feed waveguide portion as well. The feed waveguide also gives mechanical support to the probe ground plane.

The scattered electric and magnetic fields in the TE_{10} mode inside the waveguide at the $z = 0$ plane, are:

$$H_x^{10} = A_1 Y_{10}^e \sin\left\{\frac{\pi}{2a}(x + a)\right\} \tag{11}$$

$$E_y^{10} = A_1 \sin\left\{\frac{\pi}{2a}(x + a)\right\} \tag{12}$$

The time average power flowing through the waveguide is given by:

$$P = \iint \vec{E}^{10} \times \left(\vec{H}^{10}\right)^{*} dx\, dy \tag{13}$$

where the integration is carried out over the waveguide cross section. The expression for z-directed power, on carrying out the integration, is obtained as:

$$P = -2ab\, Y_{10}^{e} A_1 A_1^{*} \tag{14}$$

Since, most measuring devices have an input impedance of 50 Ohms, the voltage measured by these is given by:

$$V_m = \sqrt{50 \times P} \;\; Volts \tag{15}$$

provided the guide transporting this power is well matched with the measuring device.

This is the voltage at the probe for an incident electrical field of strength $\cos\theta_0$ Volt/meter. The antenna factor of the sensor is then given by [1, 11],

$$\mathrm{AF} = \frac{\cos\theta_0}{V_m} m^{-1} \tag{16}$$

2.3 Accounting for Wall Thickness

All window have some finite thickness, which can be accounted for by introducing higher order modes in the short section of the waveguide, formed by the window cut on the plate [2, 3]. The cross-section of the thick window sensor is shown in Figure 3. Particularly Figure 3(b) is instructive enough to show that in this case, two boundary conditions, one each at the two planes of discontinuity, are required to describe the problem completely. The analysis in this case is similar to the analysis of a thick radiating window [3].

- The incident fields are described by Equations 5 and 6, with $\phi_0 = \pi/2$.
- The assumptions presented in Section A are also applicable here.
- The aperture electric fields at the window interfaces are described by:

$$\vec{E}_{ap}(x', y', 0) = \begin{cases} \hat{u}_y \displaystyle\sum_{p=1}^{M} A_p^{\mathrm{I\ or\ II}} \sin\frac{p\pi}{2l}(x+l) & -l \le x \le l. \\ & -w \le y \le w. \\ 0 & \text{elsewhere} \end{cases} \tag{17}$$

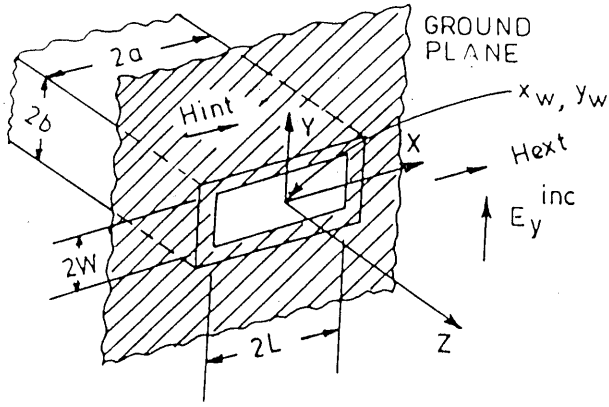

Figure 3(a). Front view of a window sensor.

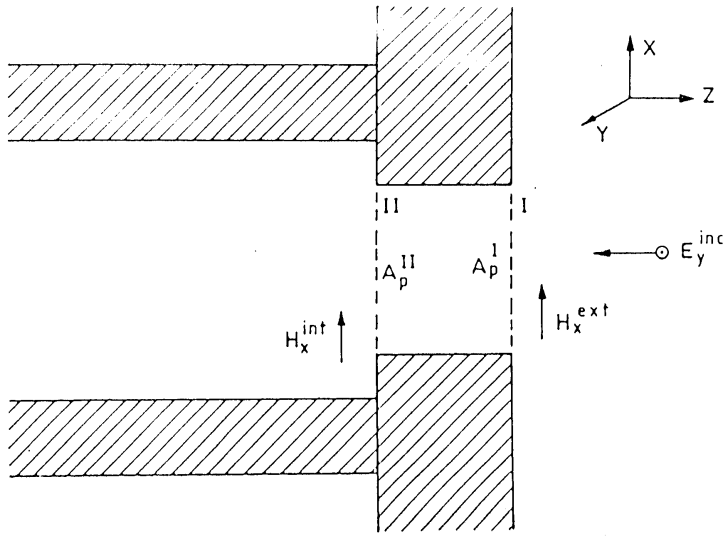

Figure 3(b). Side view of a thick window sensor.

- The internal and external scattered field are analogous to Section A.
- The scattered field inside the cavity formed by the thick wall of the window is obtained by evaluating the Cavity Green's function of the electric vector potential and they are:
  H_x due to aperture II,

$$H_x = j\frac{4}{\omega\mu}\sum_p \frac{\gamma_{po}^2}{\gamma_{po}} A_p^y \frac{\cosh\{\gamma_{po}(t-z)\}}{\sinh\{\gamma_{po}t\}} \sin\frac{p\pi}{2l}(x - x_w + l) \tag{18}$$

  and H_x due to Aperture I,

$$H_x = -j\frac{4}{\omega\mu}\sum_p \frac{\gamma_{po}^2}{\gamma_{po}} A_p^y \frac{\cosh\{\gamma_{po}Z\}}{\sinh\{\gamma_{po}t\}} \sin\frac{p\pi}{2l}(x - x_w + l) \tag{19}$$

- The boundary conditions at the interfaces I and II respectively are derived in a manner analogous to Section A.

$$2H_x^{inc\ \mathrm{I}} + H_x^{ext\ \mathrm{I}}\left(A_p^{\mathrm{I}}\right) = H_x^{cav\ \mathrm{I}}\left(A_p^{\mathrm{I}}\right) + H_x^{cav\ \mathrm{I}}\left(A_p^{\mathrm{II}}\right) \tag{20}$$

$$H_x^{int\ \mathrm{II}}\left(A_p^{\mathrm{II}}\right) = H_x^{cav\ \mathrm{I}}\left(A_p^{\mathrm{I}}\right) + H_x^{cav\ \mathrm{II}}\left(A_p^{\mathrm{II}}\right) \tag{21}$$

- The weighting functions are given by Equation 10.
- Taking moments of the terms of Equations 20 and 21 with the weighting functions converts the equations to matrix equations.
- The elements of the incident moment matrix needs special mention in this case and they are:

$$L_q^{inc} = \left\langle H_x^{inc}, w_q \right\rangle = \begin{cases} -\dfrac{8wl}{q\pi} Y_0 \cos\theta_0 \sin c(wk\sin\theta_0) : & q \text{ odd} \\ 0 & \text{otherwise} \end{cases} \tag{22}$$

- The time average power flowing through the waveguide takes the form:

$$P = \frac{2w^2l^2}{ab} Y_{10}^e \left[\sum_{p=1}^{M} A_p^{\mathrm{II}} \left[\cos\left\{\frac{\pi}{2}\left(\frac{-x_w}{a} + p - 1\right)\right\} \sin c \right.\right.$$
$$\left.\left. \cdot \left\{\frac{\pi l}{2}\left(\frac{p}{l} - \frac{1}{a}\right)\right\} - \cos\left\{\frac{\pi}{2}\left(\frac{x_w}{a} + p + 1\right)\right\} \sin c \right.\right.$$

$$\cdot\left\{\frac{\pi l}{2}\left(\frac{p}{l}+\frac{1}{a}\right)\right\}\Bigg]\Bigg]$$
$$\cdot\left[\sum_{p=1}^{M} A_p^{\mathrm{II}*}\left[\cos\left\{\frac{\pi}{2}\left(\frac{-x_w}{a}+p-1\right)\right\}\sin c\right.\right.$$
$$\cdot\left\{\frac{\pi l}{2}\left(\frac{p}{l}-\frac{1}{a}\right)\right\}-\cos\left\{\frac{\pi}{2}\left(\frac{x_w}{a}+p+1\right)\right\}\sin c$$
$$\left.\left.\cdot\left\{\frac{\pi l}{2}\left(\frac{p}{l}+\frac{1}{a}\right)\right\}\right]\right] \tag{23}$$

- The antenna factor is obtained from the relation given in Equation (16).

2.4 Dielectric Plugged Open-ended Waveguide Sensor

The sensor is shown in Figure 4. As is apparent from the diagram, the analysis of this sensor is straight forward, if the analysis for the open-ended waveguide sensor and the thick window sensor are combined effectively. The dielectric plug can be modeled as a waveguide cavity and its analysis is identical to the airfilled cavity provided by the window thickness. So, the brief sketch of the analysis procedure will be sufficient here.

The aperture field is given by

$$\vec{E}_{ap}(x',y',o)=\begin{cases}\hat{u}_y\displaystyle\sum_{p=1}^{M} A_p^{\mathrm{I\ or\ II}}\sin\frac{p\pi}{2a}(x+a) & -a\le x\le a.\\ & -b\le y\le b.\\ 0 & \text{elsewhere}\end{cases} \tag{24}$$

- The incident field is given by Equation 6.
- The internal and external field is similar to Section A.
- The scattered field inside the dielectric cavity is given by

$$H_x^{ca\nu\ \mathrm{I}}\left(A_{p_y}^{\mathrm{I}}\right)=j\frac{4}{w\mu}\sum_p A_{p_y}^{\mathrm{I}}\frac{\gamma_{po}^2}{\gamma_{po}}coth\left(\gamma_{po}t\right)\sin\frac{p\pi}{2a}(x+a) \tag{25}$$

$$H_x^{ca\nu\ \mathrm{I}}\left(A_{p_y}^{\mathrm{II}}\right)=j\frac{4}{w\mu}\sum_p A_{p_y}^{\mathrm{II}}\frac{\gamma_{po}^2}{\gamma_{po}}\cos ech\left(\gamma_{po}t\right)\sin\frac{p\pi}{2a}(x+a) \tag{26}$$

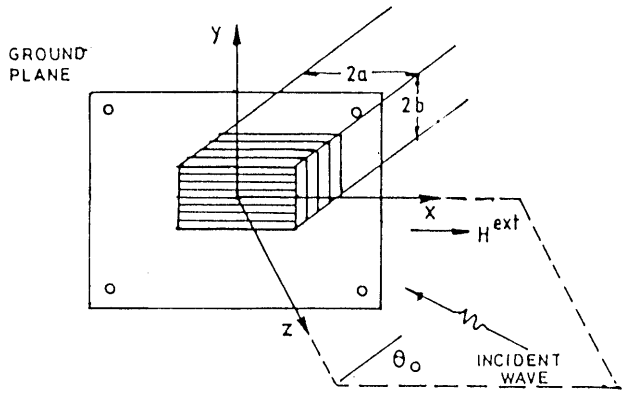

Figure 4(a). Front view of a dielectric plugged open-ended waveguide sensor.

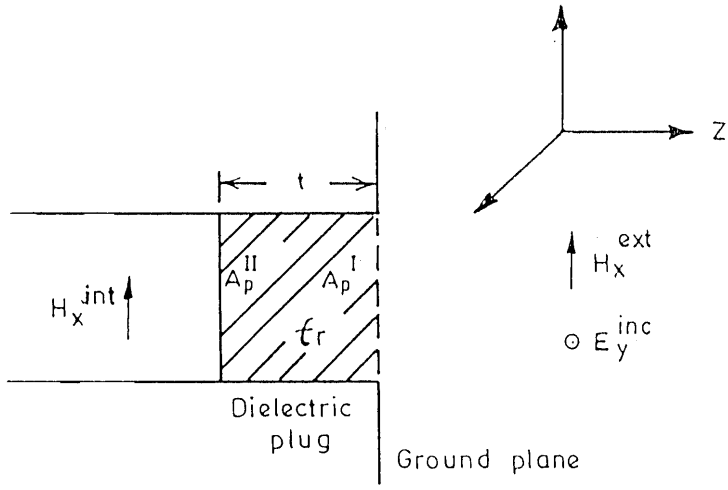

Figure 4(b). Side view of a dielectric plugged open-ended waveguide sensor.

- The boundary condition is analogous to Equations 20 and 21.
- The weighting function is obtained from Equation 10 after specializing it to open-ended waveguide case.
- The solution of the aperture field is fairly straightforward and enumerated in detail in previous sections.

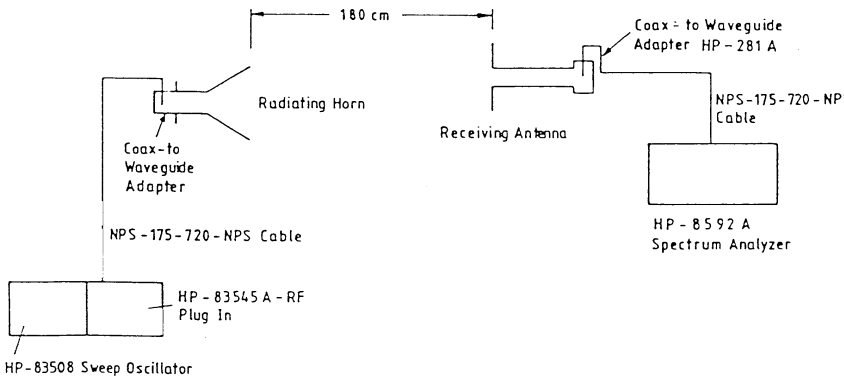

Figure 5. Experimental setup used to measure antenna factor.

- The time average dominant mode power flow is similar to Equation 14.
- The expression for antenna factor is same as Equation 16.

3. EXPERIMENTAL AND NUMERICAL RESULTS

Open-ended WR-90 waveguide, a resonant thick window and a dielectric backed open-ended WR-90 waveguide, all with a ground plane, are used as probes to sense the electric field radiated by a horn. The experimental setup used is shown in Figure 5. First, a measured amount of power at the chosen frequency is radiated by the transmitting horn, using a synthesized source. The receiving probe, in this case, an open-ended waveguide, or a window or a dielectric backed open-ended waveguide, is aligned to receive the transmitted field in the flat lobe of the transmitting antenna's radiation pattern. The position of the receiving antenna is varied, so that its elevation varies, while azimuth is kept fixed. The receiving antenna is moved along a circular path, so that it is always at a fixed distance from the transmitting antenna. The strength of the electric field at the plane of the aperture of the receiving antenna is calculated using well-known relations, and the received power is measured by a Spectrum Analyzer. Since, the standard gain horn was not available over the frequency range of interest, initially, two identical horns were used—one as the transmitter and the other as the receiver—to determine the gain of the horns by the two antenna method of measurement.

Ideally speaking, the antenna factor of any probe should be measured in Anechoic or Semi-Anechoic Chamber to limit the influence of undesired echoes in the frequency band of interest. In the experiment conducted, this effect was minimized by using microwave absorbers in the vicinity of the transmitting and receiving antennas, and by using a Spectrum Analyzer to measure the received power at the frequency of measurement.

The horn used was of size 14 cm × 12 cm × 19.3 cm (slant length). The experiment was carried out over the frequency range of 8 GHz to 12.4 GHz in steps of 0.2 GHz, with the following probes:

- Open-ended waveguide with 11 cm × 10 cm ground plane.
- Thick window of dimension $2l = 1.51$ cm, $2w = 0.5$ cm, $x_w = 0.0$, $y_w = 0.0$, $t = 1.6$ mm backed by WR-90 guide and ground plane of 11 cm × 10 cm size.
- Open-ended WR-90 waveguide with dielectric plug of thickness 8.08 mm and 9.51 mm, $\varepsilon_r = 2.63$ and a ground plane of 11 cm × 10 cm size.

The loss due to the transmitter and receiver side cables and coaxial to waveguide adapters were first determined using the HP 8757C Scalar Network Analyzer. The gain G, of the transmitting horn was next determined by using two identical horns as transmitter and receiver respectively and measuring their power by spectrum analyzer. The gain of the horn can be calculated as:

$$G = \frac{4\pi R}{\lambda}\sqrt{\frac{P_R}{P_T}} \tag{27}$$

where P_T and P_R are the transmitted and received power respectively and R the distance between the two identical horns. In the experiment performed, R was kept equal to 180 cm. These calibration data are presented in Tables 1 and 2. Also the return loss offered by different subsystems of Transmission Channel is presented in Table 3 to get an idea of the impedance mismatch existing along the path of the incoming signal.

Once the calibration is over, the transmitted power and the power received by the sensor was measured using a HP 8592A Spectrum Analyzer. Loss due to the connecting cables and adapters were taken into account. At each frequency, the power density at the plane of the sensor is given by,

$$P_D = \frac{P_T G}{4\pi R^2} \cos\theta_0 \tag{28}$$

where θ_0 is the angle between the axes of the transmitting and receiving antenna.

The field strength at the plane of the probe for oblique incidence can be obtained as follows:

The power falling over a small infinitesimal area of $dx' \times dy'$ induces an incident field of amplitude $|E|$ and space phase $e^{j(k_x x' + k_y y')}$.

Frequency (GHz)	Cable Loss CL_{TX} (dB)	Cable Loss CL_{RX} (dB)	Adapter Loss (dB)	Transmitted Signal Power P_T (dBm)
8.0	1.73	1.98	0.06	15.4
8.2	1.72	1.95	0.08	15.4
8.4	1.77	1.99	0.21	14.8
8.6	1.78	1.98	0.01	14.7
8.8	1.77	2.01	0.15	15.5
9.0	1.77	2.41	0.06	15.4
9.2	1.87	2.07	0.12	14.8
9.4	1.80	2.39	0.00	13.5
9.6	1.77	2.10	0.00	13.7
9.8	1.74	2.13	0.14	14.2
10.0	1.87	2.07	0.07	14.2
10.2	1.78	2.10	0.40	14.0
10.4	1.83	2.18	0.21	13.1
10.6	1.83	2.10	0.10	13.7
10.8	1.84	2.12	0.19	13.8
11.0	1.87	2.29	0.21	14.5
11.2	1.89	2.18	0.26	15.2
11.4	1.93	2.20	0.10	13.8
11.6	1.95	2.24	0.13	14.2
11.8	1.99	2.33	0.09	14.9
12.0	2.00	2.57	0.02	14.7
12.2	2.23	2.62	0.29	15.2
12.4	2.20	2.81	0.00	15.2

Table 1. Calibration for cable and adapter loss.

Frequency (GHz)	Power Received by the Horn (dBm)	$20\log(\lambda/4\pi R)$ (dB)	Gain of Horn G (dB)	Received Power Desity (dBm/ m^2)	Field Strength at Plane of Probe (V/m)
8.0	−4.46	−55.61	17.91	17.15	4.422
8.2	−4.37	−55.82	18.07	17.29	4.494
8.4	−5.00	−56.03	18.22	16.71	4.204
8.6	−3.71	−56.24	18.92	17.51	4.610
8.8	−3.54	−56.44	18.78	18.03	4.894
9.0	−3.03	−56.63	19.13	18.37	5.089
9.2	−3.81	−56.82	19.17	17.75	4.739
9.4	−4.31	−57.01	19.60	17.00	4.347
9.6	−4.50	−57.19	19.50	17.10	4.397
9.8	−4.27	−57.37	19.52	17.48	4.594
10.0	−4.06	−57.55	19.68	17.71	4.717
10.2	−4.00	−57.72	20.06	17.56	4.636
10.4	−5.31	−57.89	19.85	16.64	4.170
10.6	−4.60	−58.05	19.93	17.43	4.567
10.8	−5.09	−58.22	19.76	17.27	4.484
11.0	−4.30	−58.38	19.90	18.09	4.928
11.2	−3.86	−58.53	19.87	18.71	5.296
11.4	−4.70	−58.69	20.15	17.75	4.739
11.6	−4.73	−58.84	20.02	17.99	4.872
11.8	−3.88	−58.98	20.15	18.86	5.385
12.0	−4.21	−59.13	20.12	18.70	5.286
12.2	−3.49	−59.27	20.44	19.25	5.632
12.4	−2.89	−59.42	20.67	19.77	5.980

Table 2. Calculation of the gain of the transmitting horn.

So, total power incident on the probe in terms of incident field is,

$$P_R = \int_{-l}^{l}\int_{-w}^{w} \frac{\left\{|E|e^{j(k_x x' + k_y y')}\right\}^2}{\eta} dx'dy'$$
$$= 4wl\frac{|E|^2}{\eta}\sin c(2k_x l)\sin c(2k_y w) \tag{29}$$

where η is the impedance of free space $(\approx 120\pi)$. In our experiment, we kept $\phi_0 = \pi/2$. So,

$$P_R = 4wl\frac{|E|^2}{\eta}\sin c(2kl\sin\theta_0) \tag{30}$$

$$P_D = \frac{P_R}{4wl} = \frac{|E|^2}{\eta}\sin c(2kl\sin\theta_0) \tag{31}$$

Now, the incident field in terms of transmitted power is obtained by

equating the R.H.S. of Equations 28 and 31,

$$|E| = \sqrt{\frac{P_T G \eta \cos\theta_0}{4\pi R^2 \sin c(2kl\sin\theta_0)}} \tag{32}$$

The voltage at the sensor terminals, V_m, can be calculated from the measured power, P_M, assuming a matched measuring device with an input impedance of 50 ohms for the Spectrum Analyzer, using the relationship,

$$V_m = \sqrt{50 \times P_M} \tag{33}$$

The measured antenna factor is then given by,

$$AF = \frac{|E|}{V_m} m^{-1} \tag{34}$$

$$= 20\log(|E|/V_m)\, dB \tag{35}$$

The experimentally obtained data are presented in Figures 6 and 7. The frequency response of the antenna factor of the probes is taken at normal incidence to minimize the experimental errors.

Frequency (GHz)	Return Loss of Waveguide to Coaxial Adapter HP X281A (dB)	Return Loss of Cable NPS-175-720-NPS (dB)
8.0	−22.95	−1.32
8.4	−24.70	−1.63
8.8	−18.35	−2.2
9.2	−18.10	−2.84
9.6	−21.80	−3.8
10.0	−25.90	−3.77
10.4	−23.90	−1.70
10.8	−22.3	−2.20
11.2	−21.7	−3.60
11.6	−20.3	−4.38
12.0	−19.5	−4.7
12.4	−16.06	−4.05

Table 3. Return loss of the different transmission subsystem of the sensors.

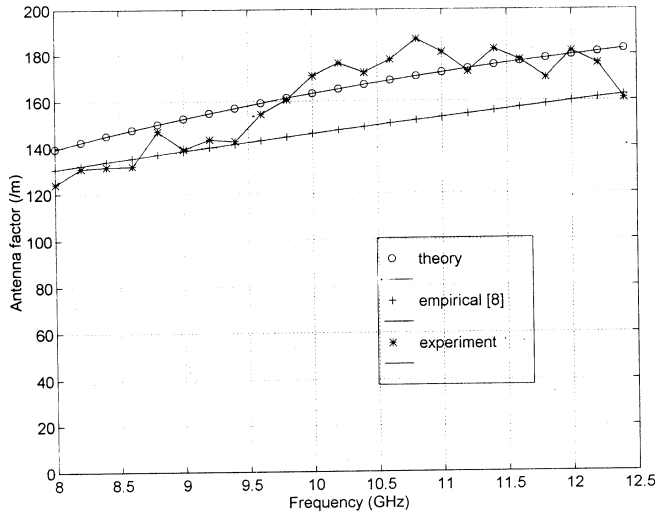

Figure 6. Variation of antenna factor with frequency for an open-ended waveguide sensor-theory, empirical formula and experiment.

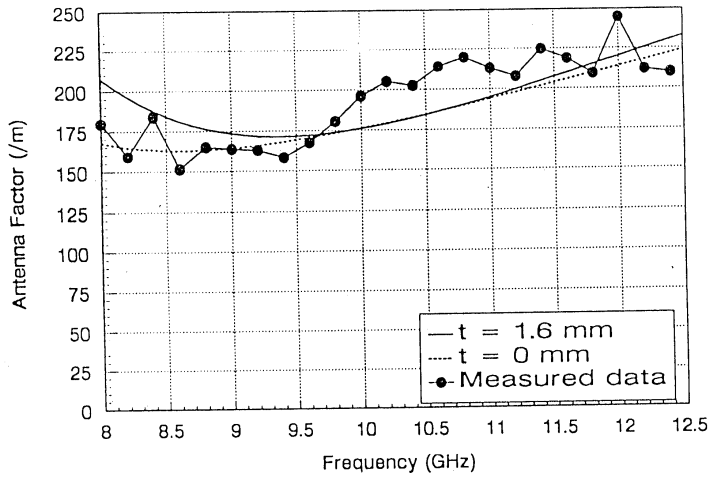

Figure 7. Variation of antenna factor with frequency for a rectangular window sensor of size $2L = 1.51$ cm, $2W = 0.5$ cm using a ground plane of 11 cm $\times$ 10 cm size-theory and experiment.

For open-ended waveguide probe, there is an empirical relation giving the gain of an antenna in transmitting as well as receiving mode, [8]

$$G = \sqrt{21.6f(2a)} \tag{36}$$

where f is the frequency in GHz, $2a$ is the larger dimension of the guide.

If only the radiation farfield is taken into account for antenna factor calculations, the antenna factor of the sensor is related to the sensor gain by the formula [8],

$$AF = \frac{9.73}{\lambda\sqrt{G}} \tag{37}$$

where λ is the free space wavelength. So,

$$AF = 46.16\sqrt{f} \tag{38}$$

is an empirical formula people use for quick calculations of antenna factor of an open-ended waveguide probe. The empirical value of the antenna factor for the open-ended waveguide probe is also plotted in Figure 6.

For the numerical calculation of the antenna factor, a software written in FORTRAN 77 was run on a Pentium 100 MHz processor based personal computer supported by LINUX operating system. The convergence criterion used for deciding the number of basis functions was chosen to be the relative percentage error committed by using a particular number of basis functions N as defined below.

$$\text{Relative error for N basis function} = \frac{\begin{array}{l}(\text{Antenna factor by taking N basis function} \\ \quad -\text{Antenna factor by taking (N}-1\text{) basis function)}\end{array}}{\text{Antenna factor by taking N basis function}} \times 100\% \tag{39}$$

The relative error along with the variation of antenna factor with N is listed in Tables 4 and 5 for open-ended waveguide and thick resonant window respectively. It is observed that for both this probes the relative error is going below 0.05% for N=11. So, all the numerical calculations of the antenna factor are carried out by taking N=11. The time taken to evaluate the antenna factor at a spot frequency by taking 11 basis function is 20 minutes for open-ended waveguide probe and 22 minutes for thick resonant window probe respectively. The number

No. of Basis Function	Antenna Factor	Relative Error (%)
1	155.37	0.57
3	156.27	0.20
5	156.58	0.10
7	156.73	0.05
9	156.82	0.03
11	156.87	0.02

Table 4. Convergence of antenna factor of the open-ended waveguide probe.

No. of Basis Function	Antenna Factor	Relative Error (%)
3	182.94	−0.14
5	182.68	−0.06
7	182.58	−0.03
9	182.52	−0.02
11	182.48	−0.01

Table 5. Convergence of antenna factor of the thick resonant window probe.

of internal waveguide modes taken in the calculations is 2500 TE as well as 2500 TM for all the other cases.

The theoretically computed antenna factor for an open-ended waveguide probe is plotted in Fig. 6. The corresponding plot for a thick resonant probe is plotted in Fig. 7. The plot for a window with zero wall thickness is also presented in the same figure. Antenna factor is also computed for the case of an open-ended waveguide sensor, where dielectric slabs of varying thickness are plugged into the open-end. The slabs are so pushed in, that their outer face flush with the ground plane. Computations are carried out for slabs with thickness $t = 8.08$ mm and 9.51 mm having a dielectric constant $\varepsilon_r = 2.63$. The computed values are presented in Figure 8.

The effect of window thickness on the antenna factor are studied in Fig. 9 for a WR90 waveguide, in which $2l/2a = 0.75$, $2w/2l = 0.5$ and t =0 mm/2 mm/4 mm/6 mm/8 mm/9 mm/10 mm/11 mm/12

mm. The data is presented over a frequency range of 8 to 12 GHz. The effect of the variation of the aspect ratio of the window on the antenna factor is presented in Fig. 10.

The antenna factor of the open-ended waveguide probe for different angle of incidence is now measured at a spot frequency of 10.01 GHz. The angle of incidence of the incoming wave is varied from 0 to 85° by varying the angle of elevation while the azimuth angle was kept fixed at $\pi/2$. The experimental data as well as theoretical data is presented in Figure 11. Due to the large variation of the values between 0° and 85°, the antenna factor is presented in dB scale. The corresponding presentation for a 1.6 mm thick resonant window having $2l = 1.51$ cm, $2w = 0.5$ cm, $x_w = y_w = 0$ is presented in Figure 12.

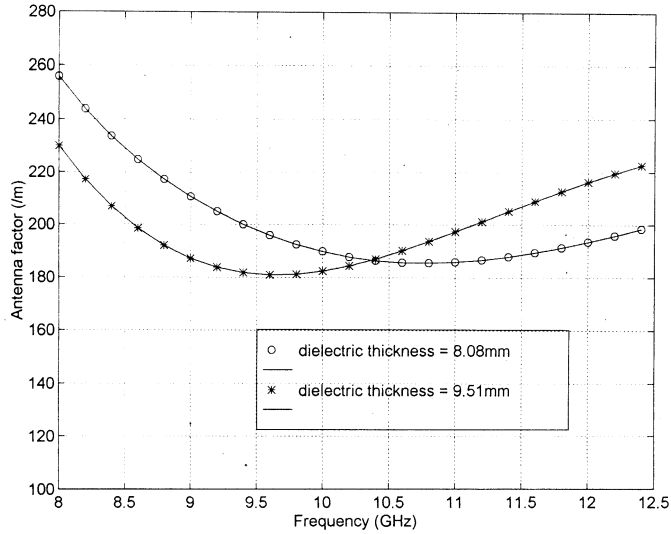

Figure 8. Antenna factor of dielectric plugged open-ended waveguide sensor.

4. DISCUSSION

For the open-ended waveguide probe and resonant window probe, Figures 6 and 7 reveal that the experimental results show a better match with the present formulation at the higher frequency band, compared to the empirical formula used by the EMC practitioners. The theoretical result using the present formulation starts showing significant

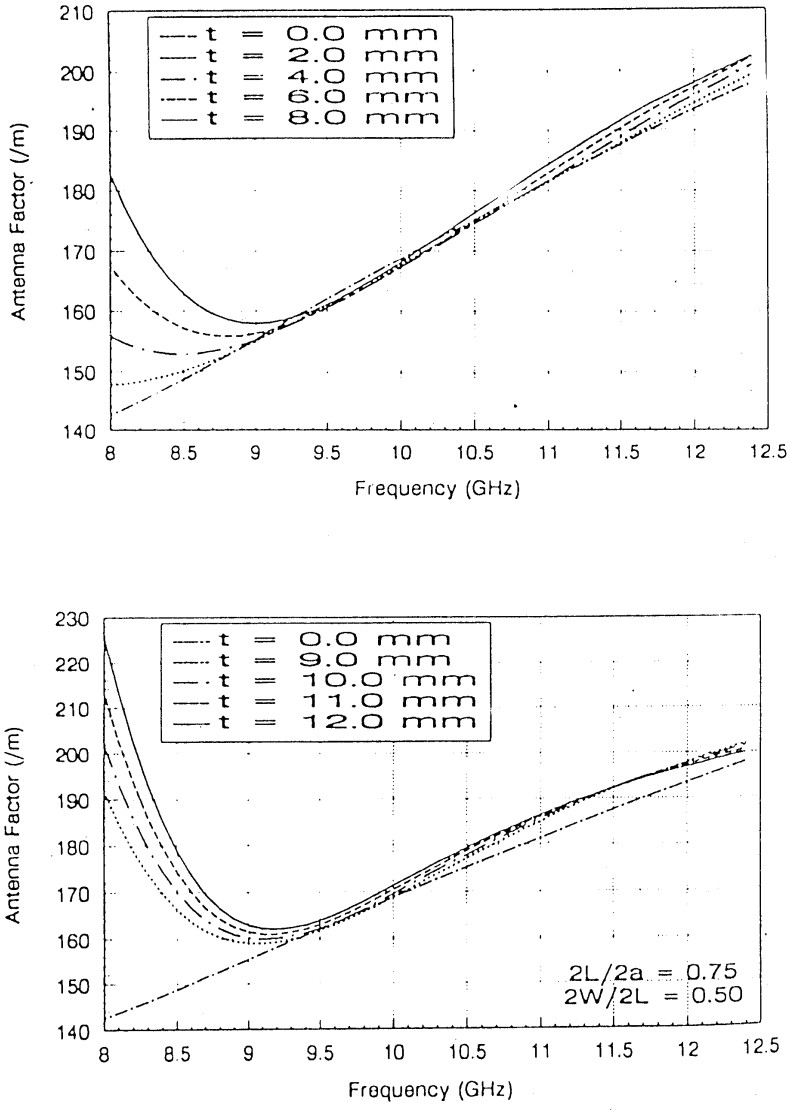

Figure 9. Antenna factor of windows with different thickness: $2L/2a = 0.75$, $2W/2L = 0.50$, $t = 0$ mm, 2 mm, 4 mm, 6 mm, 8 mm, 9 mm, 10 mm, 11 mm, 12 mm, over 8–12.4 GHz.

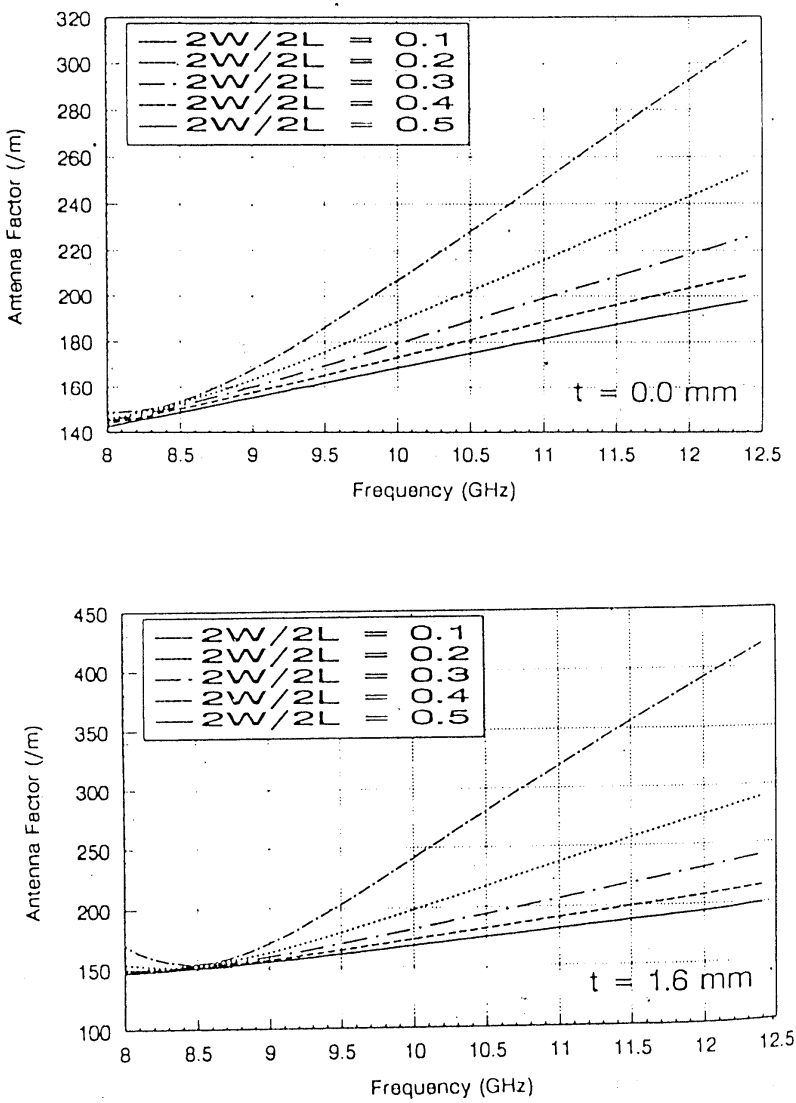

Figure 10. Antenna factor of windows with different aspect ratios: $2L/2a = 0.75$, $2W/2L = 0.1,\ 0.2,\ 0.3,\ 0.4,\ 0.5$; $t = 0$ mm/1.6 mm, over 8–12.4 GHz.

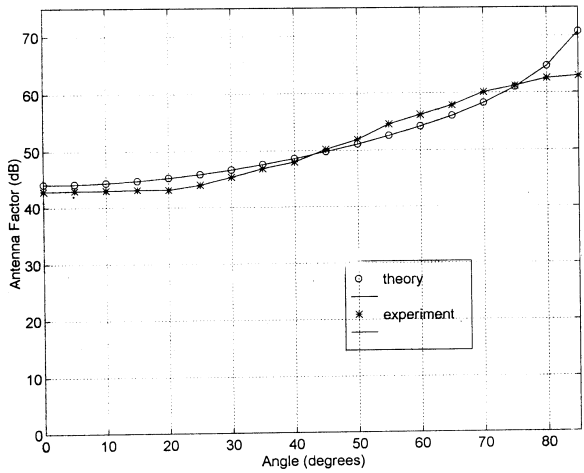

Figure 11. Variation of antenna factor with elevation angle for an open-ended waveguide sensor.

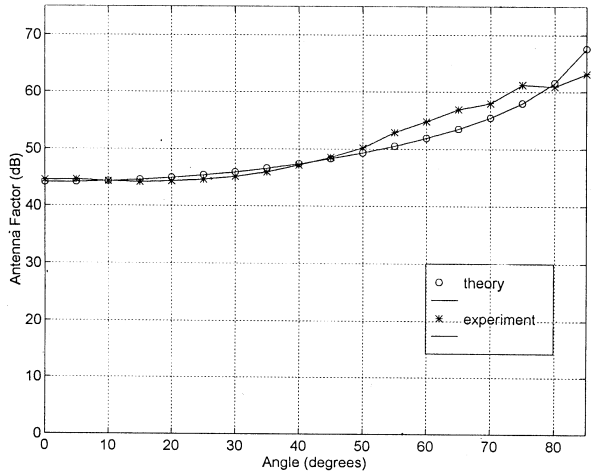

Figure 12. Variation of antenna factor with elevation angle for a resonant window sensor.

variation from empirical formula after 10 GHz onwards. As the empirical formula assumes only farfield type fields, the deviation from the empirical formula underlines the effect of non-farfield type fields at the sensing plane of the sensor. So, the present analysis becomes more and more useful beyond 10 GHz. However, the empirical result is found to be within an accuracy of 7% for open-ended waveguide and 11% for window sensor below 10 GHz.

The agreement between present theory and measurement for the open-ended waveguide can be said to be good; however, the discrepancy is not at all negligible. To explore the possible reasons for the experimental error, an inspection of Table 3 is mandatory. It is seen that , even if one takes into account the insertion loss of cable and adapters into the measurement, the mismatch produced by the cable will contribute to the measurement error significantly. The standing waves created by this cable mismatch and also to some extent by the adapter mismatch has conclusively proved that the power transported by the feeding guide is not fully dissipated at the Spectrum Analyzer load. The Spectrum Analyzer is seen to offer a $50\,\Omega$ load throughout the frequency band of operation. So, the way out is either to use a better cable or to model the impedance of the mismatched cable. Since, no better cable could obtained, and the theoretical modeling could not be carried out at the time of writing this paper, the measurement error could not be removed. The other sources of possible errors are enumerated below:

- Use of a finite ground plane in measurements although the theory is for a sensor with infinite ground plane. The assumption of zero electric field throughout the ground plane except at the aperture opening, does not hold good when the ground plane is finite in extent. However, it is seen in case of radiators that at least a ground plane of size $5\lambda \times 5\lambda$ is sufficient to simulate the effects of infinite ground plane. The ground plane used in the experiment is shorter in size than this requirement. But the motive for using short ground plane was to disturb the surrounding as little as possible. Further, the electromagnetic field scattered by structures behind the antenna may find a way into the open-end due to the presence of a finite ground plane.
- Scattering by other reflecting bodies in the vicinity, though efforts were made to minimize the same.
- Errors in calibrating the horn, cables and adapters, etc.

- Cross-polarizing components ignored in the analysis. Though for a single sensor, the cross-polarized field does not generally have any significant contribution.
- Errors in orienting the sensor with respect to the transmitting horn, particularly to keep the azimuth angle to be $\pi/2$.

It is expected that with better cables, adapters, etc. and a more controlled experimental environment where the above aspects can be taken care of, the results would show better agreement. Further, there is a contradiction for the choice of ground plane between measurement accuracy and sensor application. Measurement accuracy demands that the ground plane should be as large as possible, whereas for EMI measurements, the attempt would to disturb the ambient electric field as little as possible. An open-ended waveguide with a small ground plane, or preferably without any ground plane should ideally be used for such measurements.

The results presented for the resonant window probe show that in this case the agreement between theory and experiment is worse than in the case of open-ended waveguide. Apart from the sources of error already pointed out, the possibility of the presence of the air gap between the ground plane and the plate containing the window, could have contributed significantly to the error. The trend of experimental data, however, agrees well with the theoretical one. Also, the importance of including wall thickness in the theoretical model is clearly revealed by Figure 9, where the better match of the experimental result with the model incorporating wall thickness is self-evident.

Unlike the window or the open-ended waveguide radiator, the number of basis functions M, required for convergence is small. For all the sensors studied in this paper, convergence was obtained for $M \leq 9$. Hence, one can say that the electric field distribution at the receiving aperture is closer to the sinusoidal one compared to the case of the transmitting aperture.

Encouraged by the excellent impedance match obtained over narrow band with open-ended waveguides with dielectric plugs as transmitter [2], these devices were studied as receivers. The theoretical results obtained (Figure 8) show that as receivers, the performance of such devices is inferior to that of the simple open-ended waveguide sensor. The antenna factor of these devices is marginally better than that of the open-ended waveguide, over a small bandwidth. As receiving antennas, therefore these devices do not seem to be as encouraging,

as they are as transmitting antennas. It may sound like violating the Lorentz Reciprocity Theorem. But at second thought, it will be clear that this seeming contradiction between transmitting and receiving case is perfectly reconciled to the Principle of Reciprocity. The catch is that as a receiver, a uniform plane wave is incident on the aperture, while as a transmitter, a non-uniform plane wave (as the dominant TE_{10} mode in the waveguide is) is incident upon it from within the waveguide.

The curves presented in Figure 9 demonstrate that with increasing thickness of the window, there is a drastic increase in the antenna factor up to about 9 GHz, while above this frequency, the window thickness has marginal influence on the antenna factor. In fact, window, in general, is inferior to the open-end of a rectangular waveguide as a sensor. The thick window antenna factor has a narrow band frequency response, i.e., the usable zone of the antenna factor is comparatively low. The figure under consideration suggests the the thickness itself bring this frequency sensitivity into play, thereby reducing the effectiveness of the sensor for use as a wideband sensor. However, for detecting a weak narrowband signal in presence of broadband noise, this receiver can find application as a tuned detector.

From Figure 10, it is seen that the antenna factor of a window sensor is higher than that of the open end of a rectangular waveguide over the entire frequency range, and expectedly, with increase in the aspect ratio $(2w/2l)$ the antenna factor decreases. The plots show some interesting features. Expectedly, the power received, increased with increase in the aspect ratio, due to the larger opening presented. However, at the lower range of frequency, say, below 8.5 GHz, this increase is marginal. Further, in case of the thick windows $(t = 1.6$ mm), the difference in power received over thin windows. There is even a resonance effect near about 8.5 GHz for the thick window $(t = 1.6$ mm) with low aspect ratio (0.1, 0.2).

The variation of antenna factor data with the angle of incidence, as shown in Figure 11 and 12 show that there is a tremendous variation with angle of incidence. For small angles of incidence, say below 40°, the theory matches well with the experiment. For larger angles, the received power is too low to separate itself from the EMI noise present in the experimental environment thereby producing significant discrepancy between the theoretical and experimental data. Nevertheless, the method presented offers an excellent way for the determination of the

susceptibility of radars to undesired radiation in real life situations.

An open-ended waveguide is the best possible sensor. Any structure placed in the guide deteriorates its performance. So, while calibrating the sensors, any undesired discontinuity presented by flanges, adapters, cables etc. can contribute significantly to the experimental errors. The chances of errors are more in thick windows than in open-ended waveguide, due to the increase in number of the discontinuities. This observation can explain the significant discrepancy observed between theoretical and experimental curves in Figures 6 and 7.

The results shown in this paper conclusively proves that whereas there is much room for improving the performance of waveguide radiators by window or dielectric loading, it is a futile attempt to improve upon the performance of the open-ended waveguide sensor. So, in the fabrication of high frequency sensors, uniformity in shape and dimension should be considered as critical. The results presented, even with the relatively crude experimental setup, are encouraging enough to use the analysis to correctly predict the Antenna Factor of waveguide sensors. The theoretical prediction of the antenna factor of EMI sensors is a very attractive alternative if one takes into consideration the enormous expenditure and time required for calibrating a sensor experimentally. Also, for experimental calibration, each and every sensor is to be calibrated individually, whereas for theoretical calibration all the sensors constituting a particular type can be calibrated at one go using the same approach, it is possible to predict the susceptibility of such antennas to electromagnetic radiation incident from any direction. The aperture sensors basically sense the magnetic field at the aperture. So, they are good for low impedance fields. For high impedance fields other types of EMI sensors should be used.

REFERENCES

1. Clayton, P. R., *Introduction to Electromagnetic Compatibility,* John Wiley & Sons Inc., New York, 1992.
2. Gupta, S., A. Bhattacharya, and A. Chakraborty, "Analysis of an open-ended waveguide radiator with dielectric plug," *IEE Proceedings on MAP,* Vol. 144, No. 2, 126–130, April 1997.
3. Das, B. N., A. Chakraborty, and S. Gupta, "Analysis of waveguide fed thick radiating rectangular windows in a ground plane," *IEE Proc.,* Part H, Vol. 138, No. 2, 142–146, April 1991.

4. Raju, G. S. N., A. Chakraborty, and B. N. Das, "Studies on wide inclined slots in the narrow wall of rectangular waveguide," *IEEE Trans. on Antenna and Propagation,* Vol. 38, No. 1, 24–29, January 1990.
5. Bhattacharya, A., K. S. R. Rao, and A. Chakraborty, "Generalized analysis of thick rectangular window as EMI sensors," Asia Pacific Microwave Conference Proceedings, 1500–1503, India, 1996.
6. Gupta, S., A. Bhatacharya, and A. Chakrabory, "Analysis of thick rectangular window in the receiving mode," IEEE AP-S Proceedings, Canada, 1997.
7. Bhattacharya, A., S. Gupta, and A. Chakraborty, "Analysis of open-ended rectangular waveguide sensors for EMI measurements," Accepted in IEEE Instrumentation and Measurement Technique Conference, 1998.
8. Wu, D. I., and M. Kanda, "Comparison of theoretical and experimental data for the nearfield of an open-ended rectangular waveguide," *IEEE Trans. on EMC,* Vol. 31, 353–358, 1989.
9. Harrington, R. F., and J. R. Mautz, "A generalized network formulation for aperture problems," *IEEE Trans. on Antenna and Propagation,* Vol. 24, 870–873, Nov. 1976.
10. Harrington, R. F., *Time Harmonic Electromagnetic Fields,* McGraw Hill Book Company Ltd., New York, 1961.
11. Macnamara, T., *Handbook of Antennas for EMC,* Artech House, London, 1995.